Supporting Information for

Electric-Field Effects on Adsorbed-Water Structural and Dynamical Properties at Rutile- and Anatase-TiO_2 Surfaces

Zdenek Futera and Niall J. English**

School of Chemical and Bioprocess Engineering, University College Dublin, Belfield, Dublin 4, Ireland

* Corresponding authors: niall.english@ucd.ie, zdenek.futera@ucd.ie; Tel: +353-1-7161646 (NE), Fax: +353-1-7161177 (both)

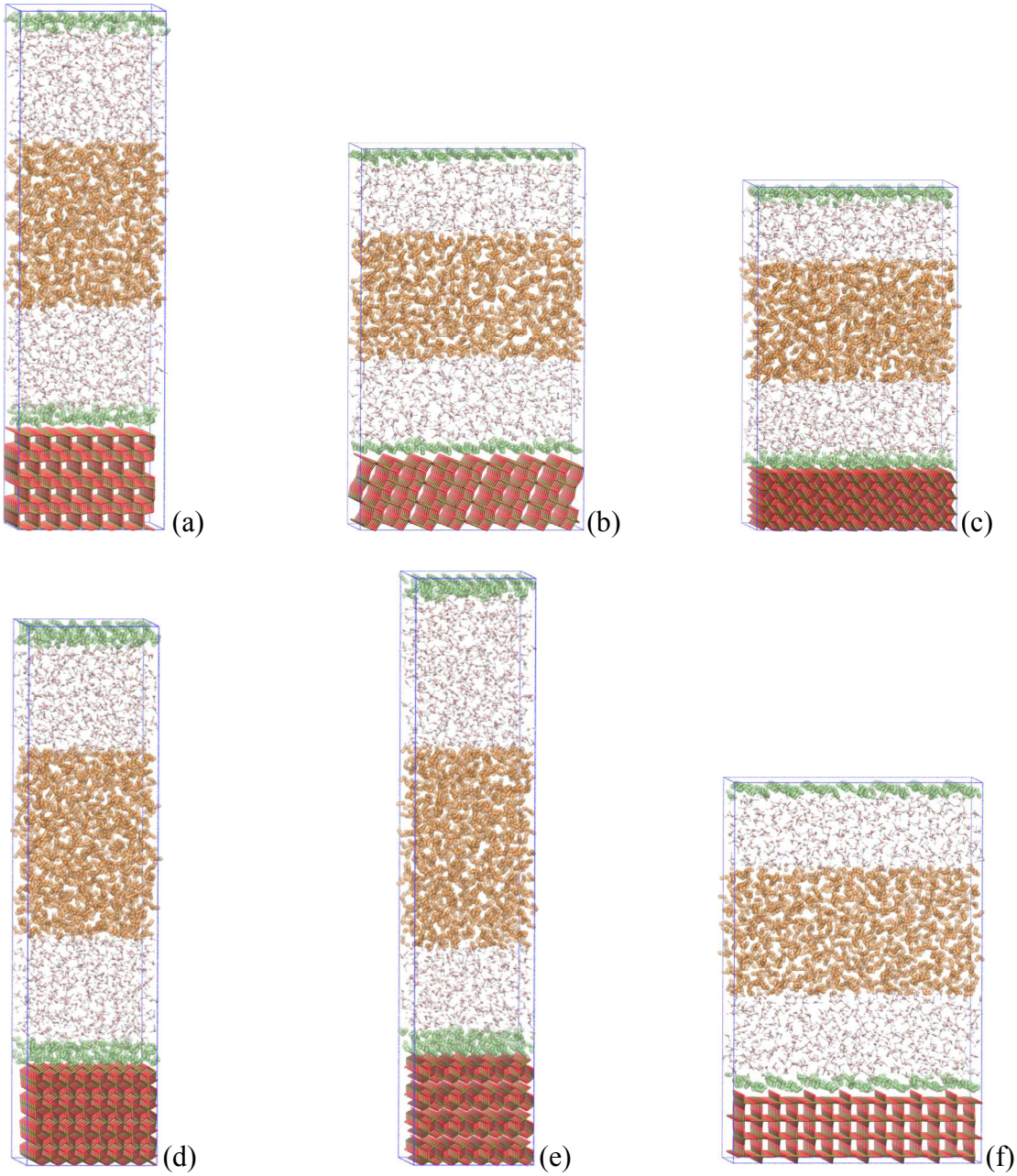

Figure S1: Supercell models of TiO_2 / water interfaces: (a) anatase (001), (b) anatase (101), (c) rutile (001), (d) rutile (100), (e) rutile (101), (f) rutile (110). The bulk-water region is highlighted by orange colour, and interface water in green.

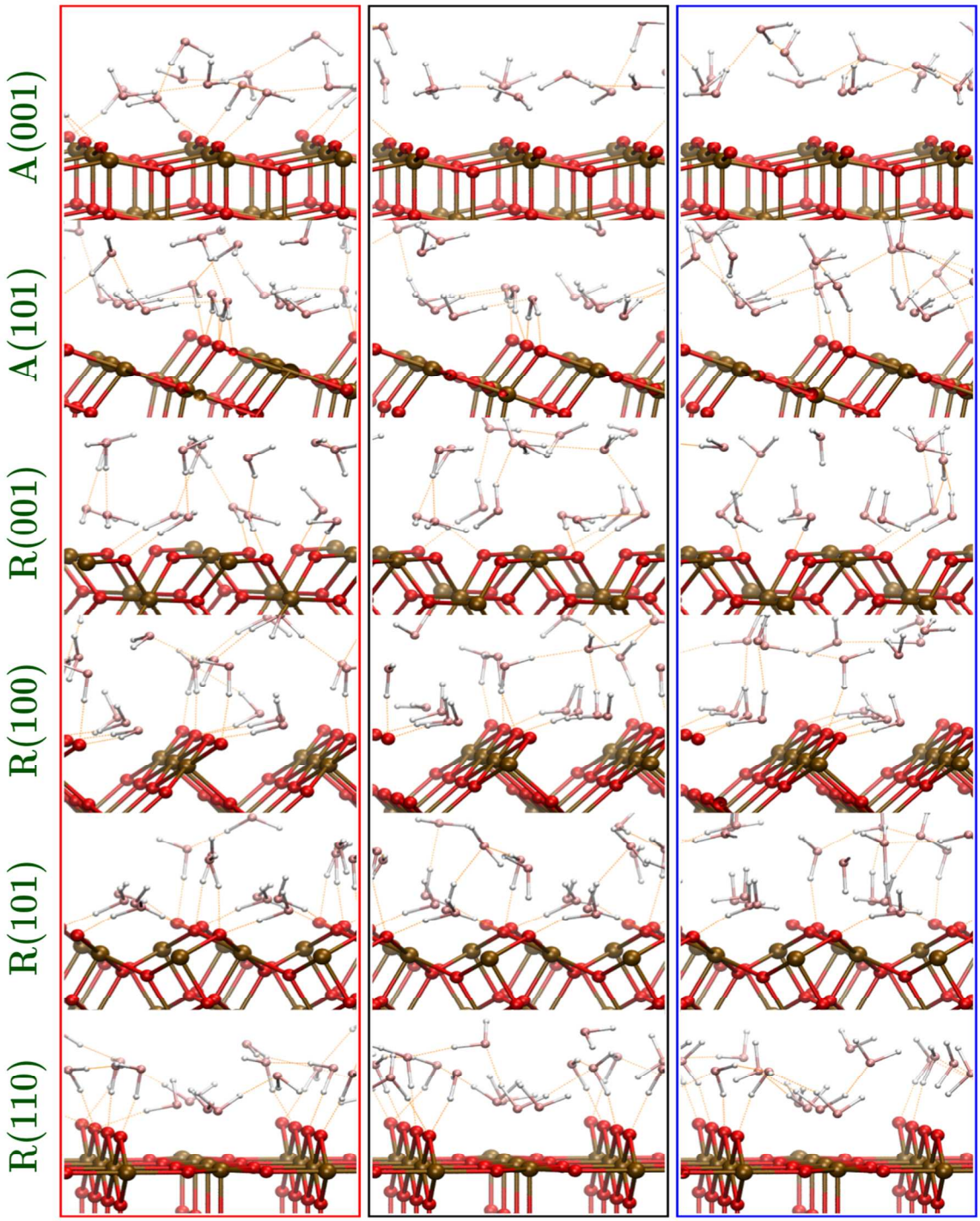

Figure S2: Snapshots of TiO_2 / water interfacial structures: Anatase (001), Anatase (101), Rutile (001), Rutile (100), Rutile (101) and Rutile (110). Zero-field structures (black frame) are compared with structures affected by external static electric field of 0.25 V/Å magnitude applied in parallel (blue frame) / anti-parallel (red frame) direction to the surface normal.

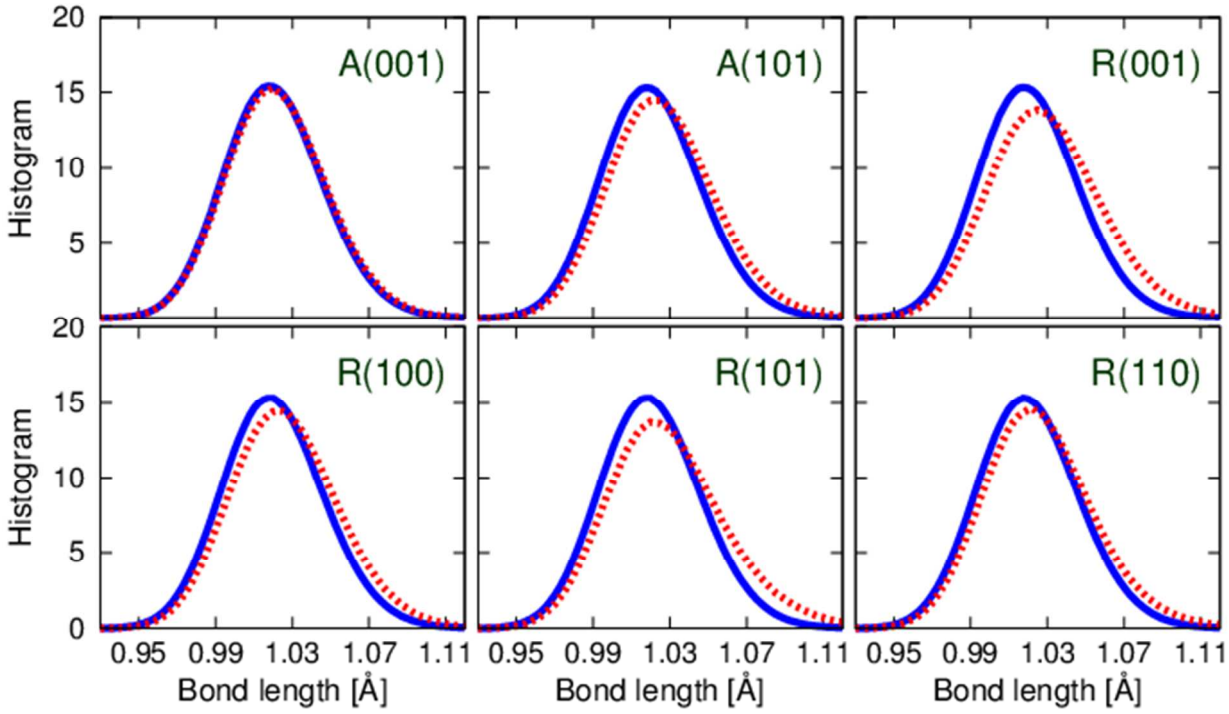

Figure S3: Distribution of O_w-H_w water bond lengths in bulk (solid blue) and in the interfacial region (dotted red) at zero-field conditions.

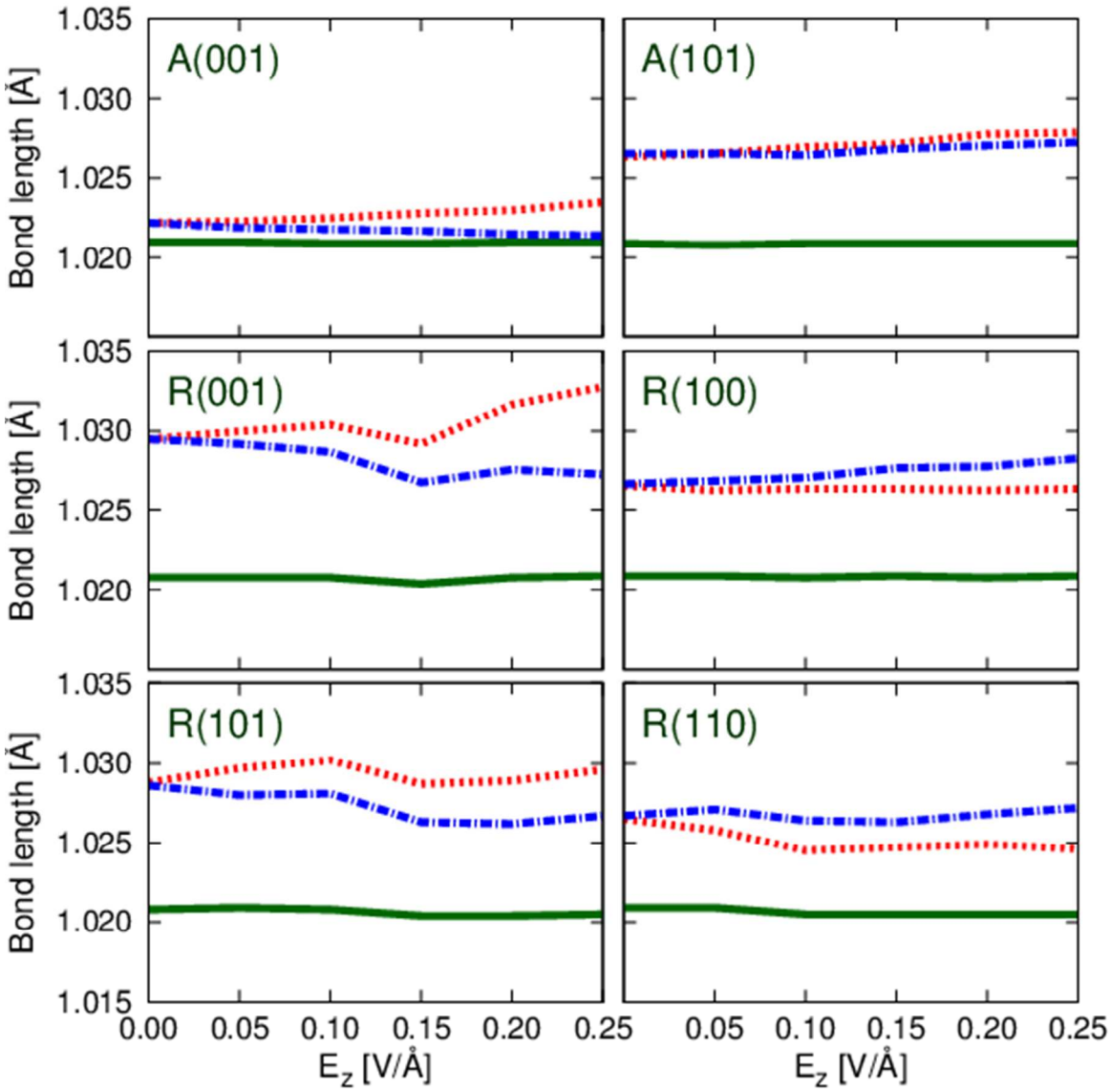

Figure S4: Mean value of O_w-H_w water-bond-length distribution in bulk (solid green), in the interface with surface normal parallel with the applied external field (dash-dot blue) and in the anti-parallel interface (dotted red) as functions of the external electric-field magnitude.

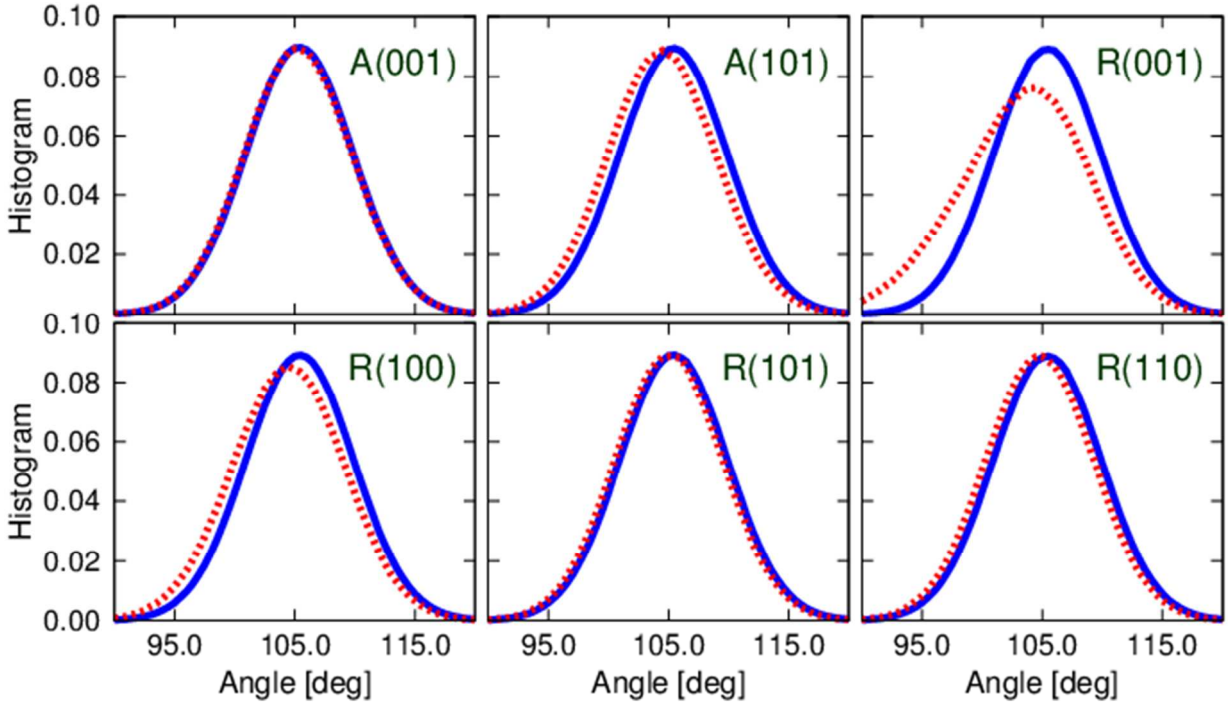

Figure S5: Distribution of H_w-O_w-H_w water valence angle in bulk (solid blue) and in the interfacial region (dotted red) at zero-field conditions.

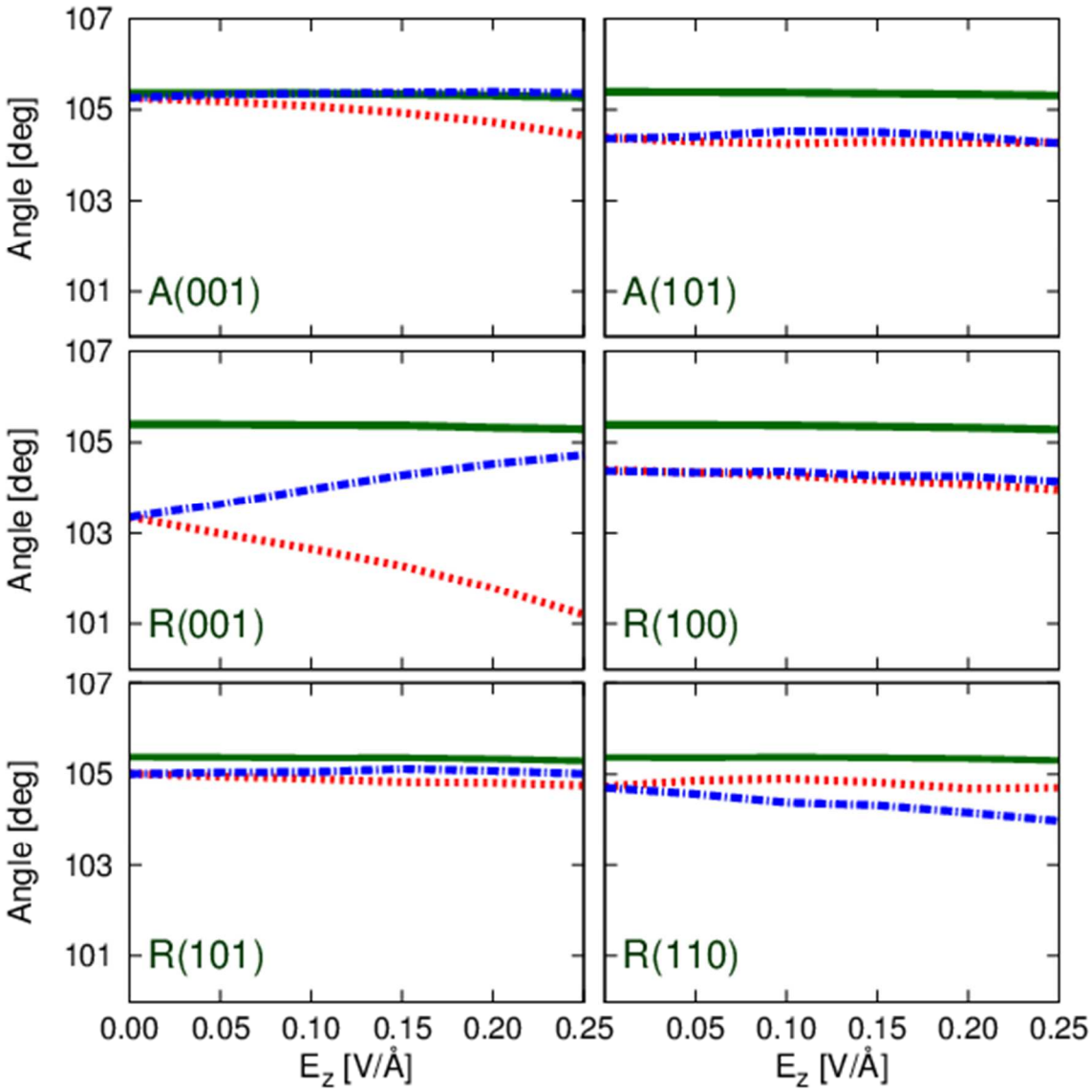

Figure S6: Mean value of H_w-O_w-H_w water valence-angle distribution in bulk (solid green), in the interface with surface normal parallel with the applied external field (dash-dot blue) and in the anti-parallel interface (dotted red) as functions of the external electric field magnitude.

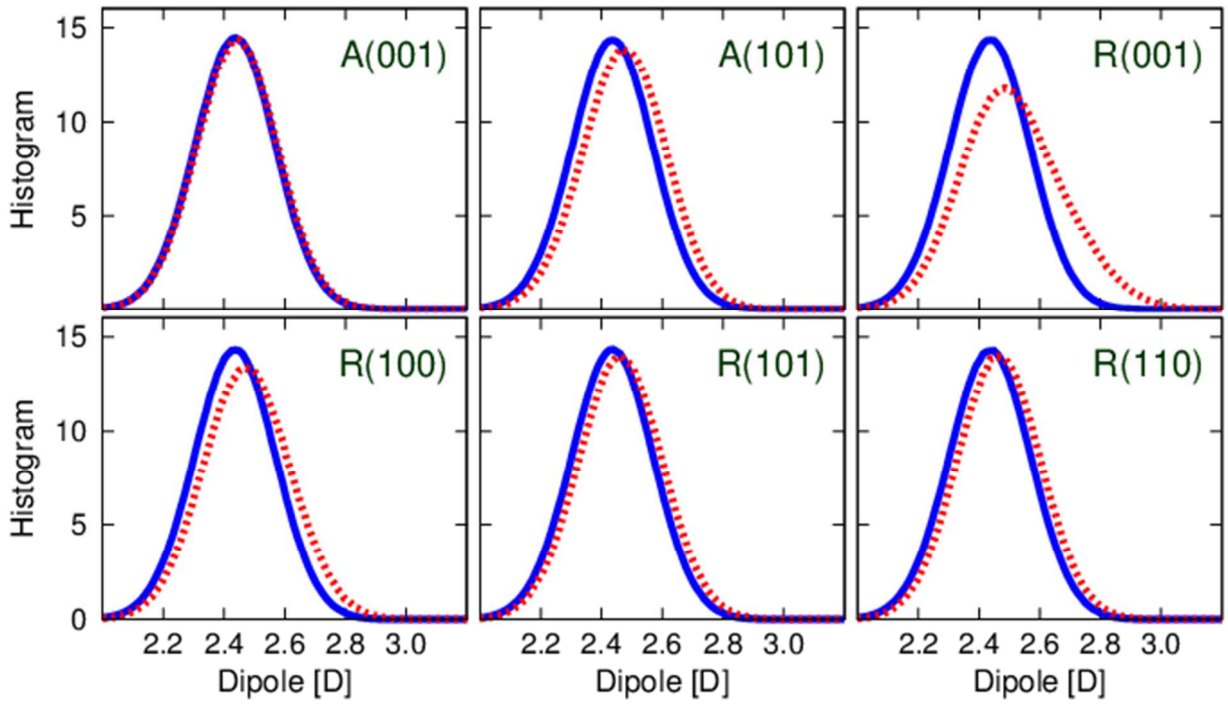

Figure S7: Distribution of water dipole moment in bulk (solid blue) and in the interfacial region (dotted red) at zero-field conditions.

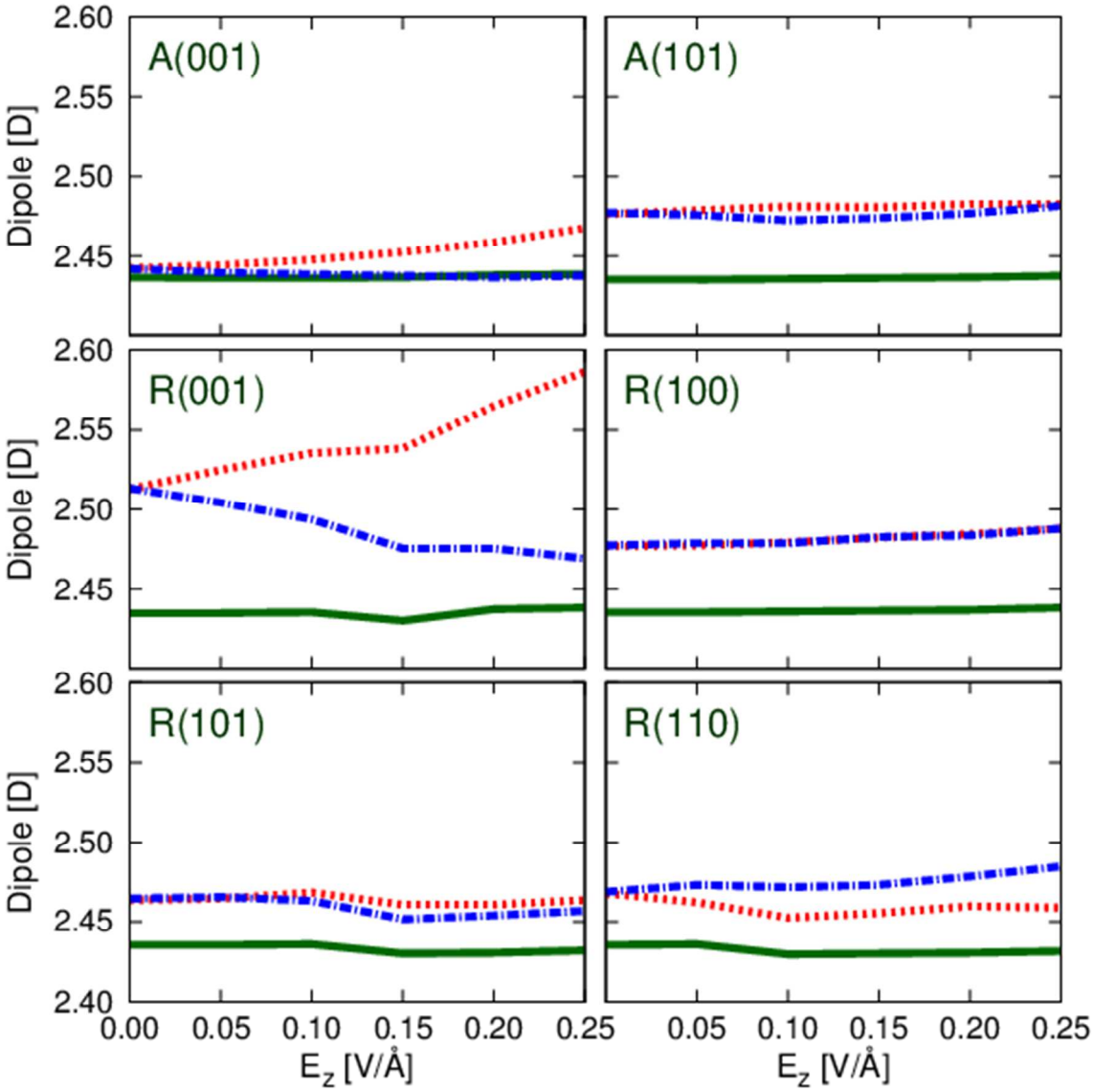

Figure S8: Mean value of water-dipole distribution in bulk (solid green), in the interface with surface normal parallel with the applied external field (dash-dot blue) and in the anti-parallel interface (dotted red) as functions of the external electric-field magnitude.

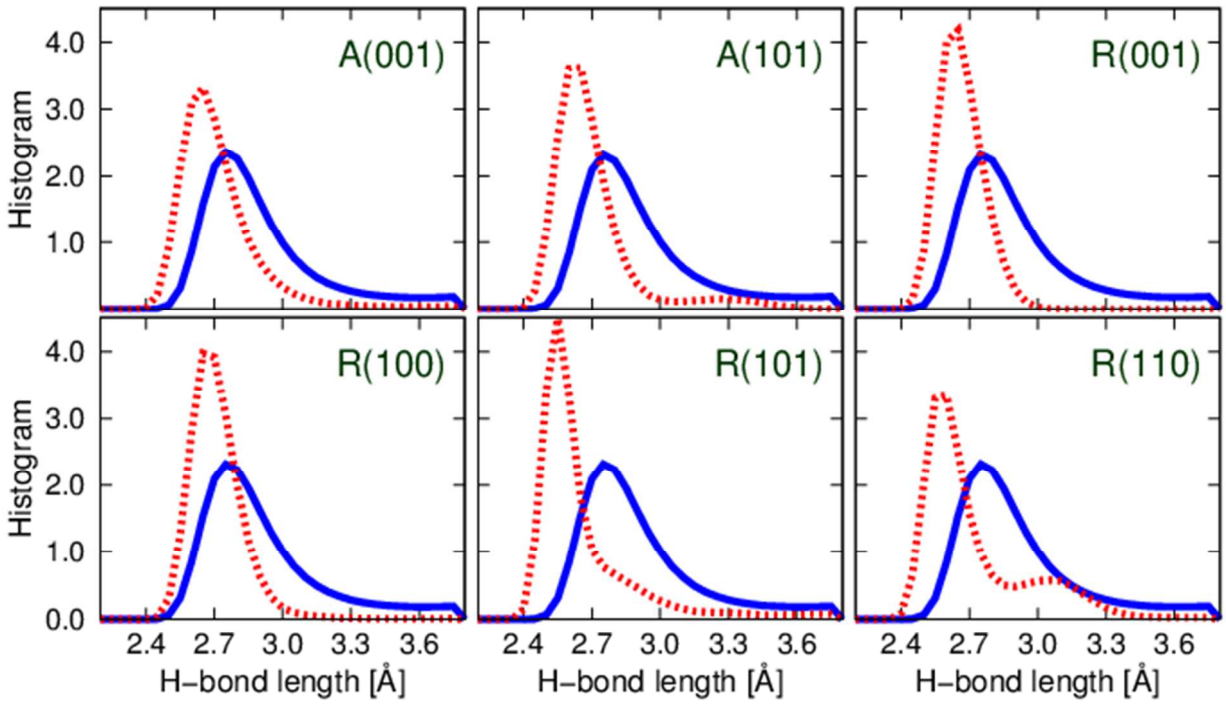

Figure S9: Distribution of hydrogen-bond donor-acceptor lengths in bulk (solid blue) and in the interfacial region (dotted red) at zero-field conditions.

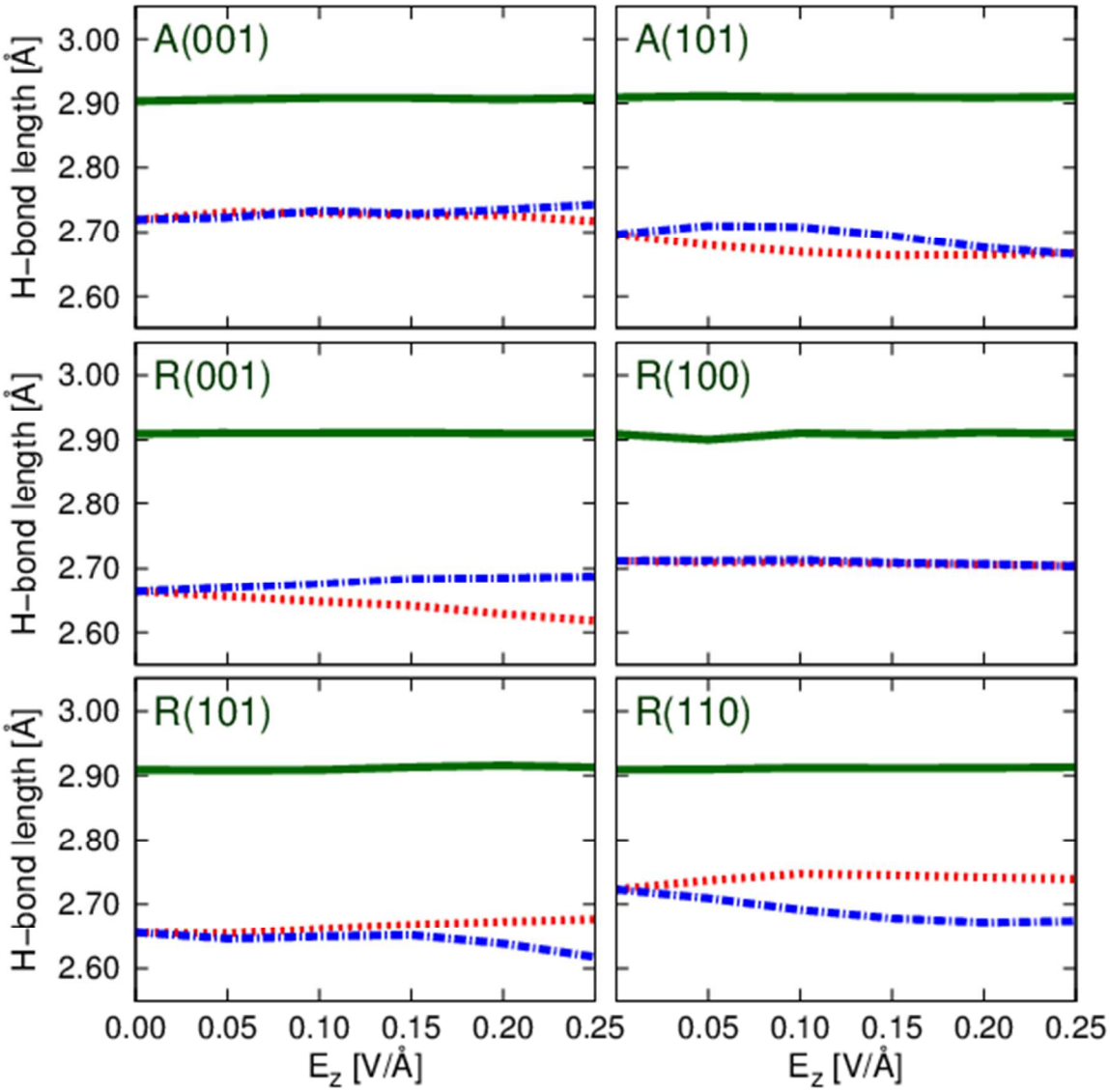

Figure S10: Mean value of hydrogen-bond donor-acceptor length distribution in bulk (solid green), in the interface with surface normal parallel with the applied external field (dash-dot blue) and in the anti-parallel interface (dotted red) as functions of the external electric-field magnitude.

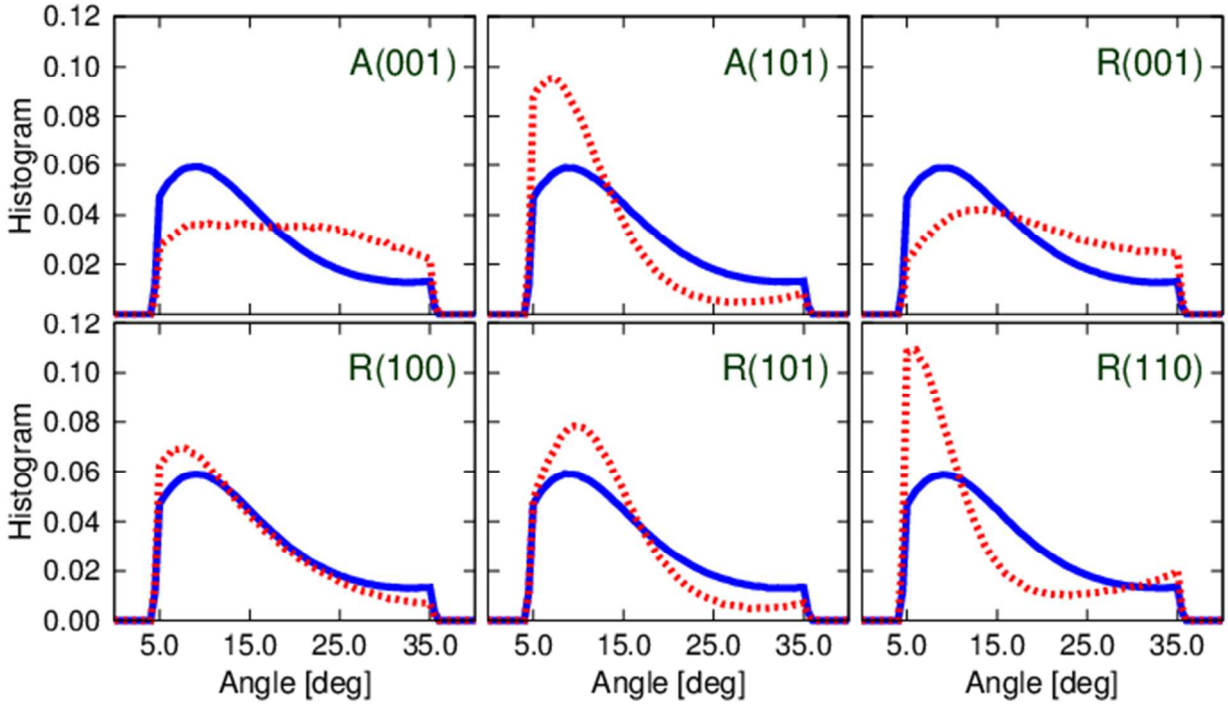

Figure S11: Distribution of hydrogen-bond A-D-H angles in bulk (solid blue) and in the interfacial region (dotted red) at zero-field conditions.

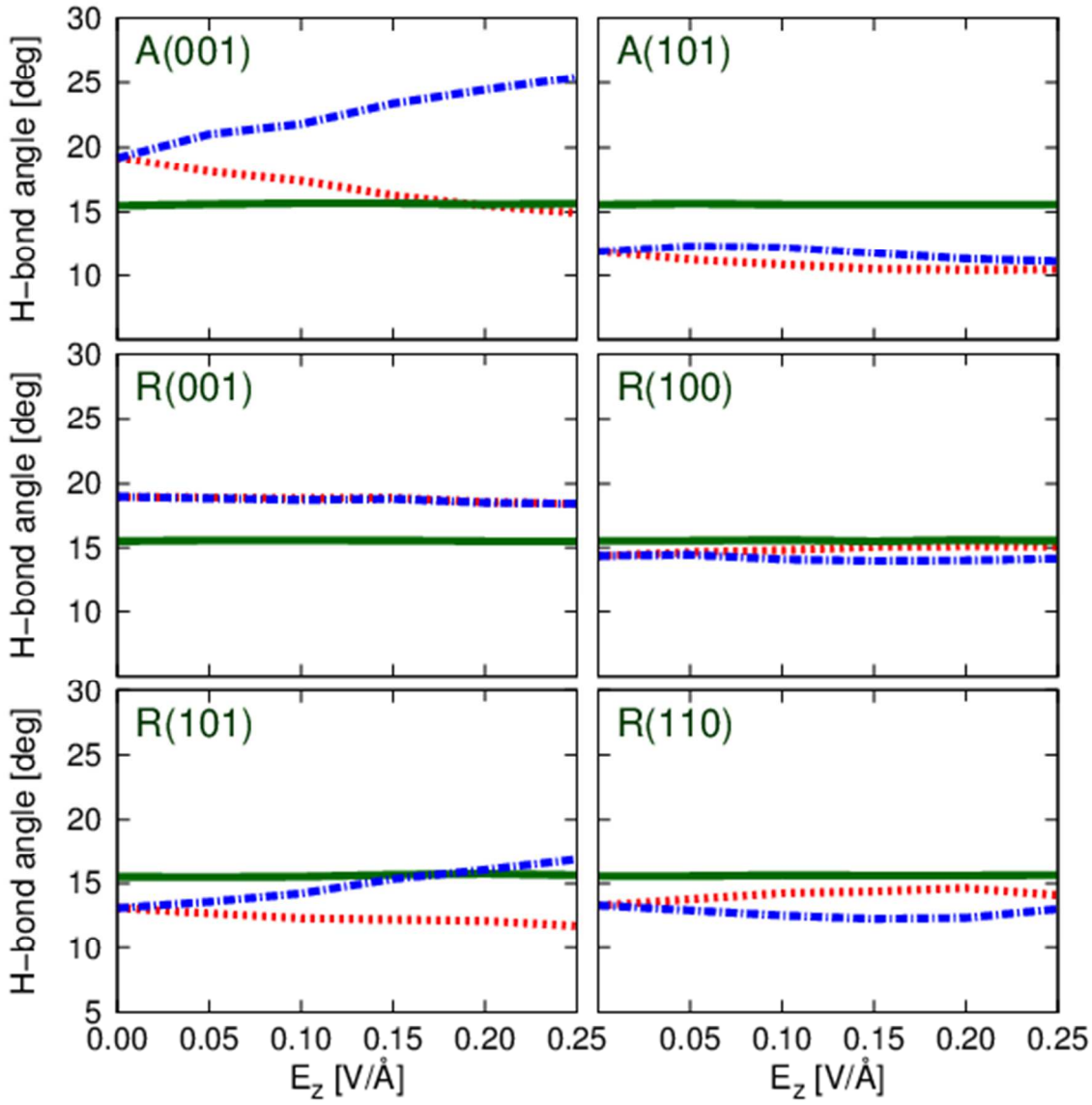

Figure S12: Mean value of hydrogen-bond angle distribution in bulk (solid green), in the interface with surface normal parallel with the applied external field (dash-dot blue) and in the anti-parallel interface (dotted red) as functions of the external electric field magnitude.

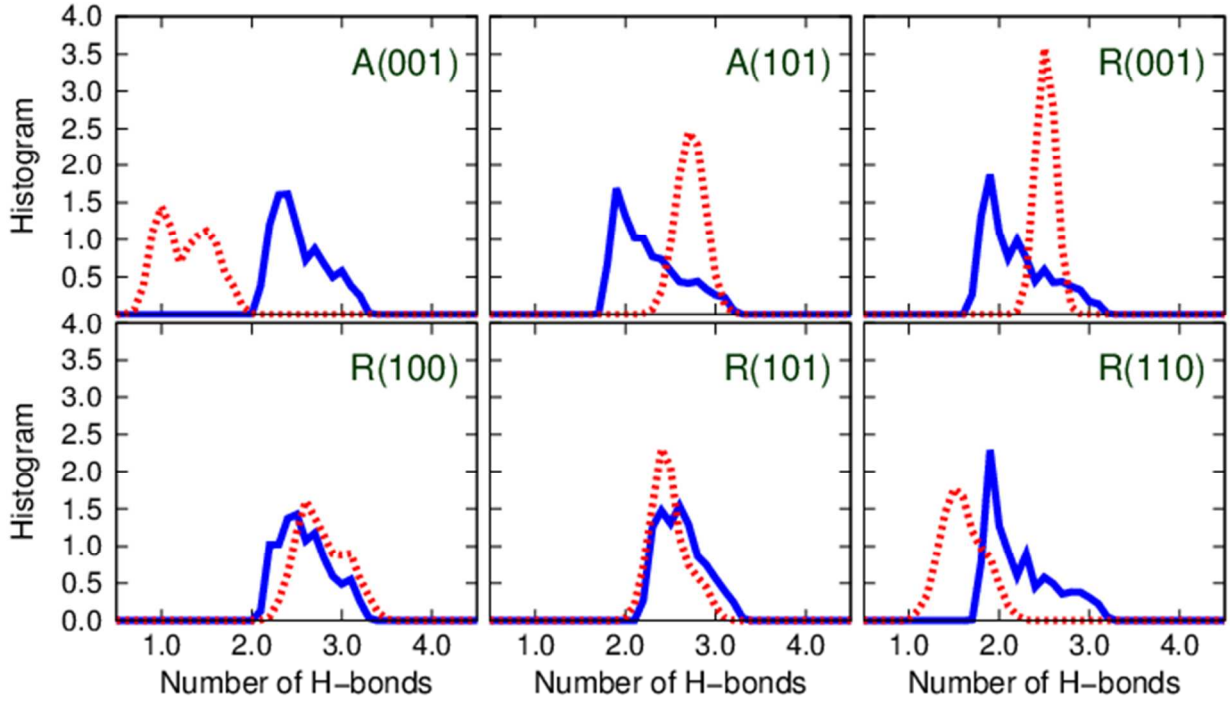

Figure S13: Distribution of average number of hydrogen bonds in bulk (solid blue) and in the interfacial region (dotted red) at zero-field conditions.

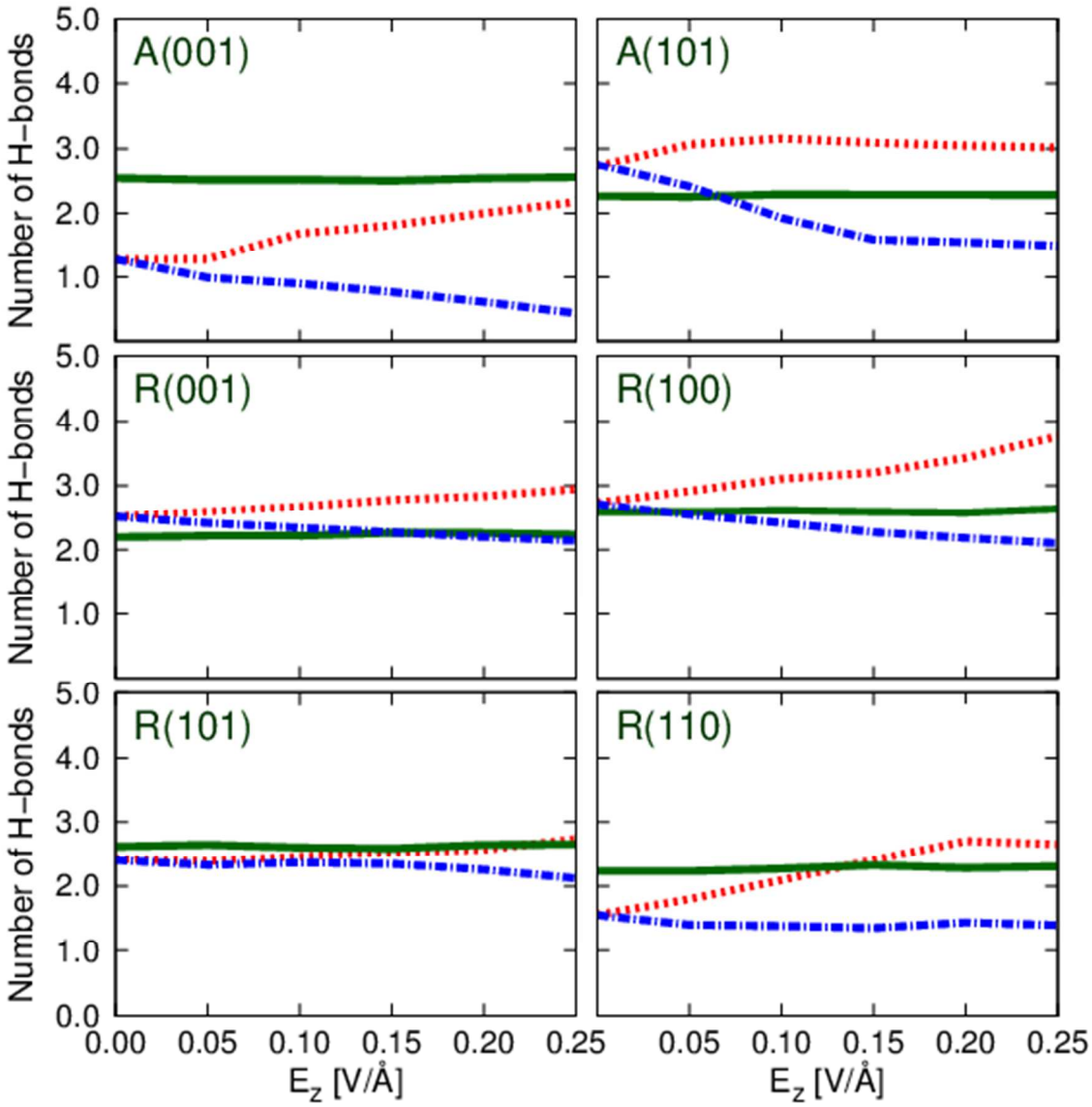

Figure S14: Mean value of distribution of average number of hydrogen bonds per one water molecule in bulk (solid green), in the interface with surface normal parallel with the applied external field (dash-dot blue) and in the anti-parallel interface (dotted red) as functions of the external electric field magnitude.

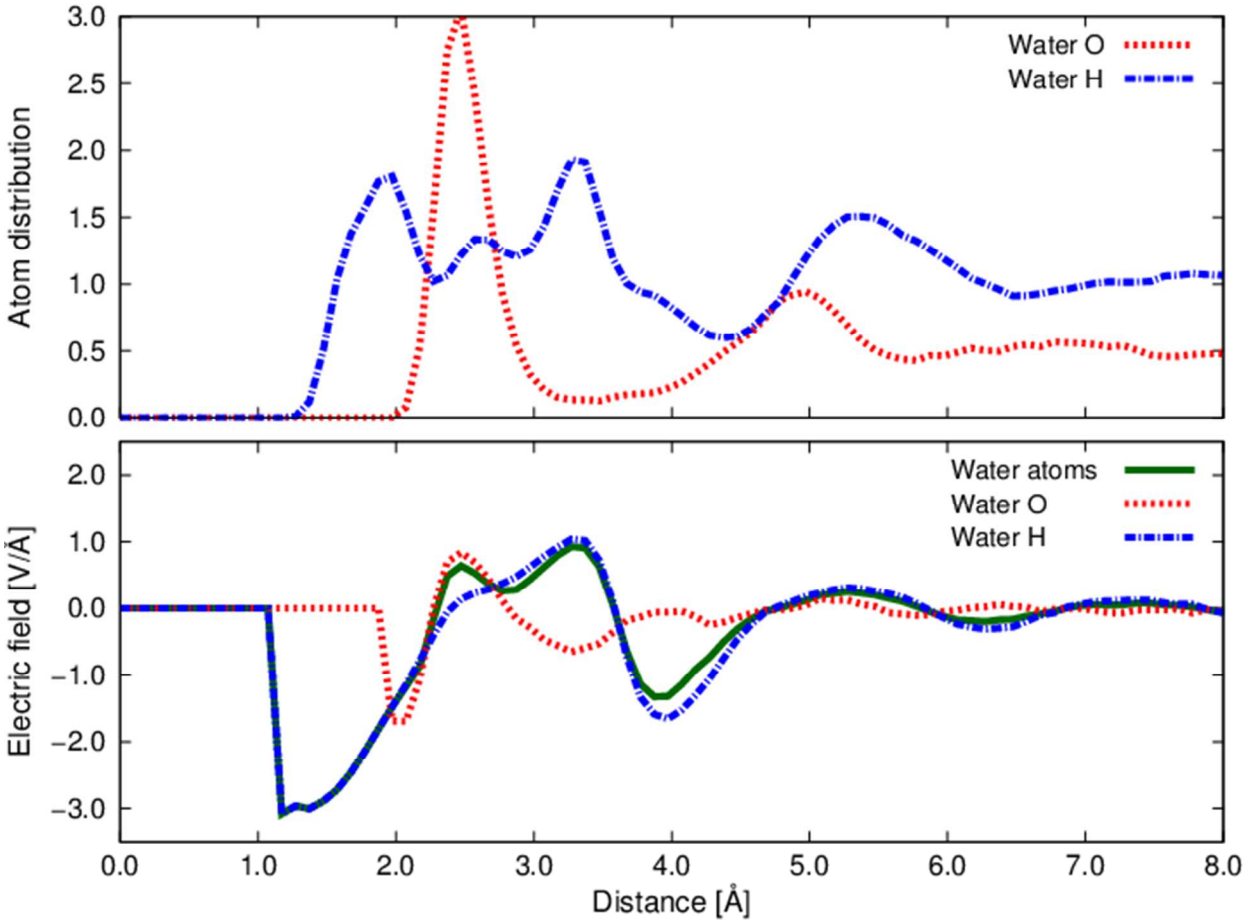

Figure S15: Water atom distribution (upper panel) and decomposition of intrinsic electric field profile to water-atom contributions (lower panel) on anatase (001) interface. Oxygen contributions are shown in dashed red line, hydrogen contributions in dash-dot blue line and and the total electric-field profile is plotted in solid green line.

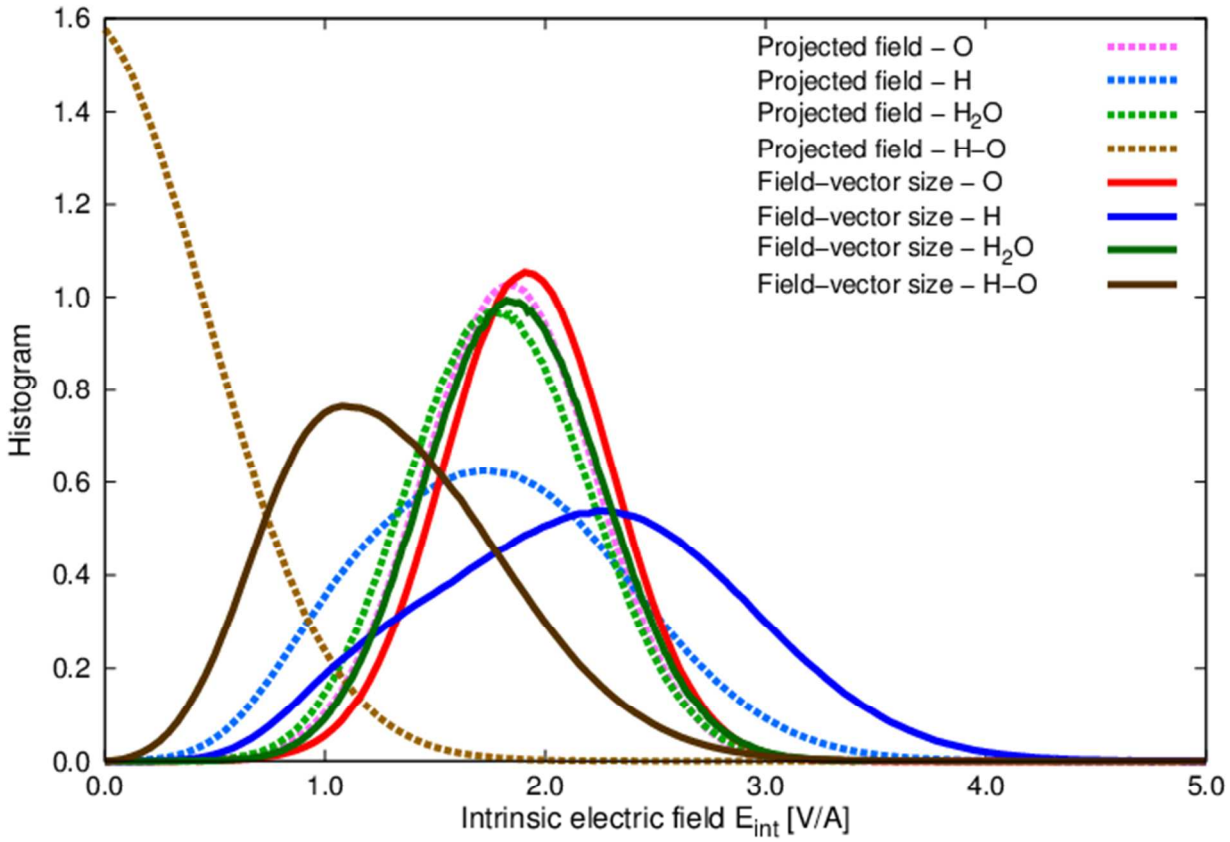

Figure S16: Comparison of total electric field vector size ($|\vec{E}| = \sqrt{\vec{E} \cdot \vec{E}}$) distribution and projected electric field vector to molecular water dipole direction ($E_\mu = \vec{e}_\mu \cdot \vec{E}$) distributions in bulk region of anatase (001) model. The field on water oxygen atoms ($\vec{E}_O$, red); hydrogen atoms ($\vec{E}_{H1}$ and $\vec{E}_{H2}$, blue); average water-molecule field ($\vec{E}_w = \frac{1}{3}(\vec{E}_O + \vec{E}_{H1} + \vec{E}_{H2})$, green) and differential H_w-O_w field ($\vec{E}_{H1} - \vec{E}_O$ and $\vec{E}_{H2} - \vec{E}_O$, brown) are plotted.

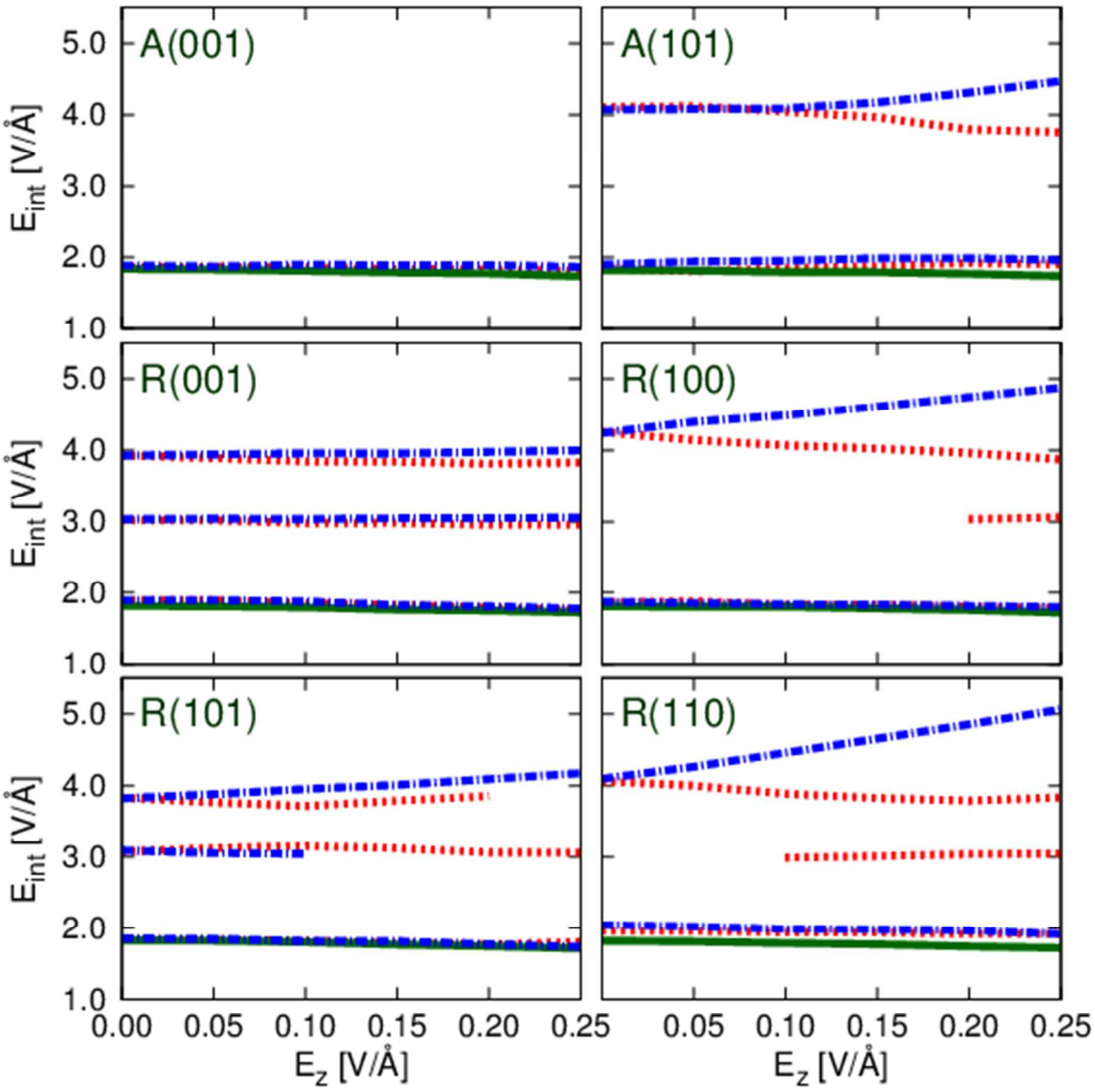

Figure S17: Peak positions of three-Gaussian fit of probability distribution of *intrinsic* electric field projected onto the water-dipole direction. Peaks in bulk (solid green), in the interface with surface normal parallel with the applied external field (dash-dot blue) and in the anti-parallel interface (dotted red) as functions of the external electric field magnitude are shown.

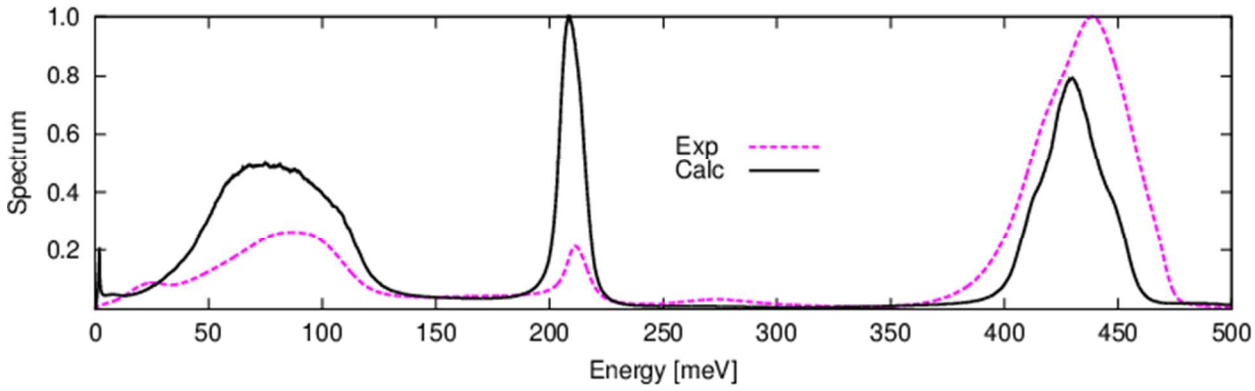

Figure S18: Comparison of calculated IR spectrum of bulk water with the experimental data.

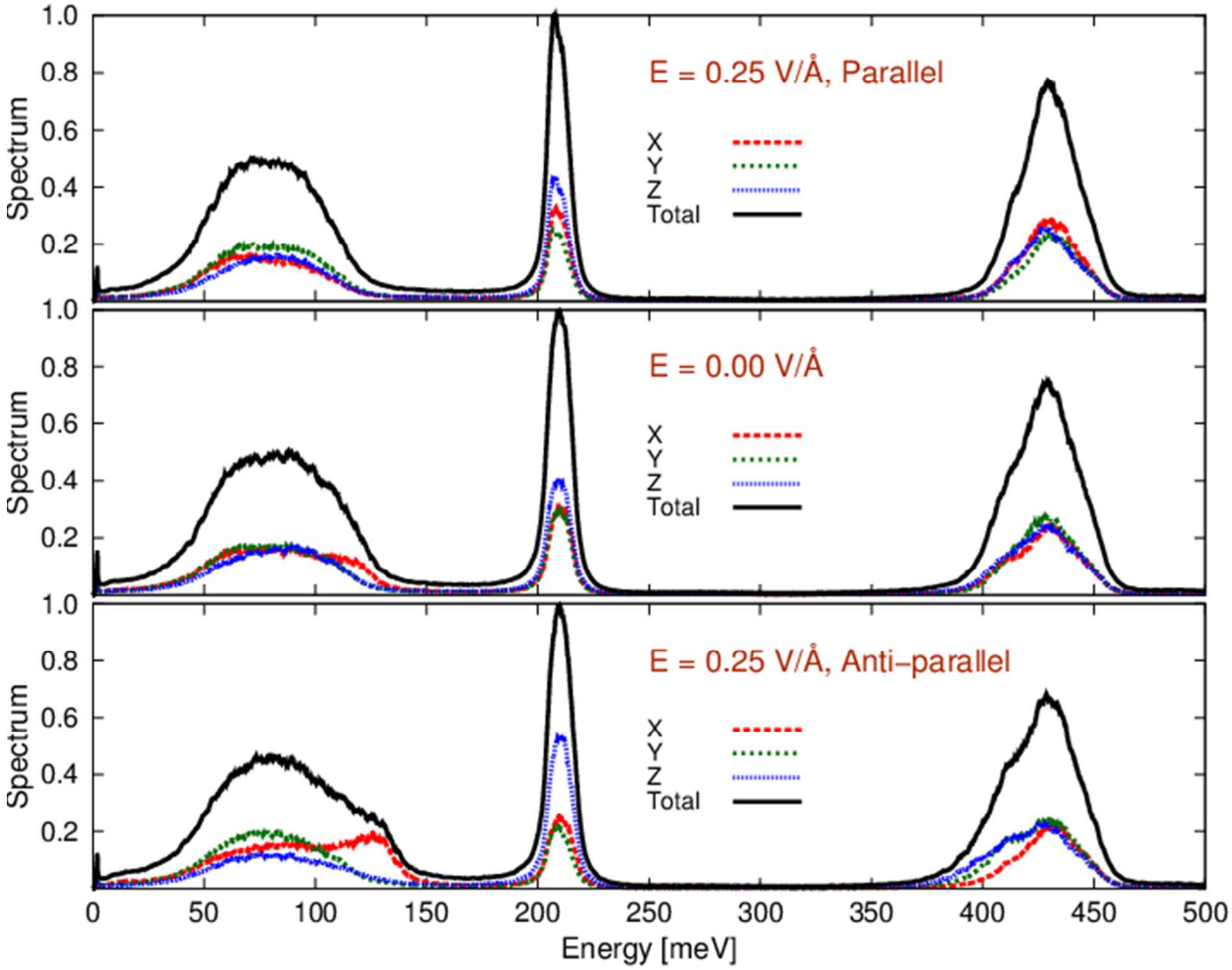

Figure S19: IR spectra of interfacial water on anatase (001) surfaces. Effects of the external static electric fields in the *z*-direction perpendical to the TiO_2 surface, parallel and antiparallel to the surface normal, are compared with the zero-field conditions. The spectra are decomposed to simulation-cell coordinate system.

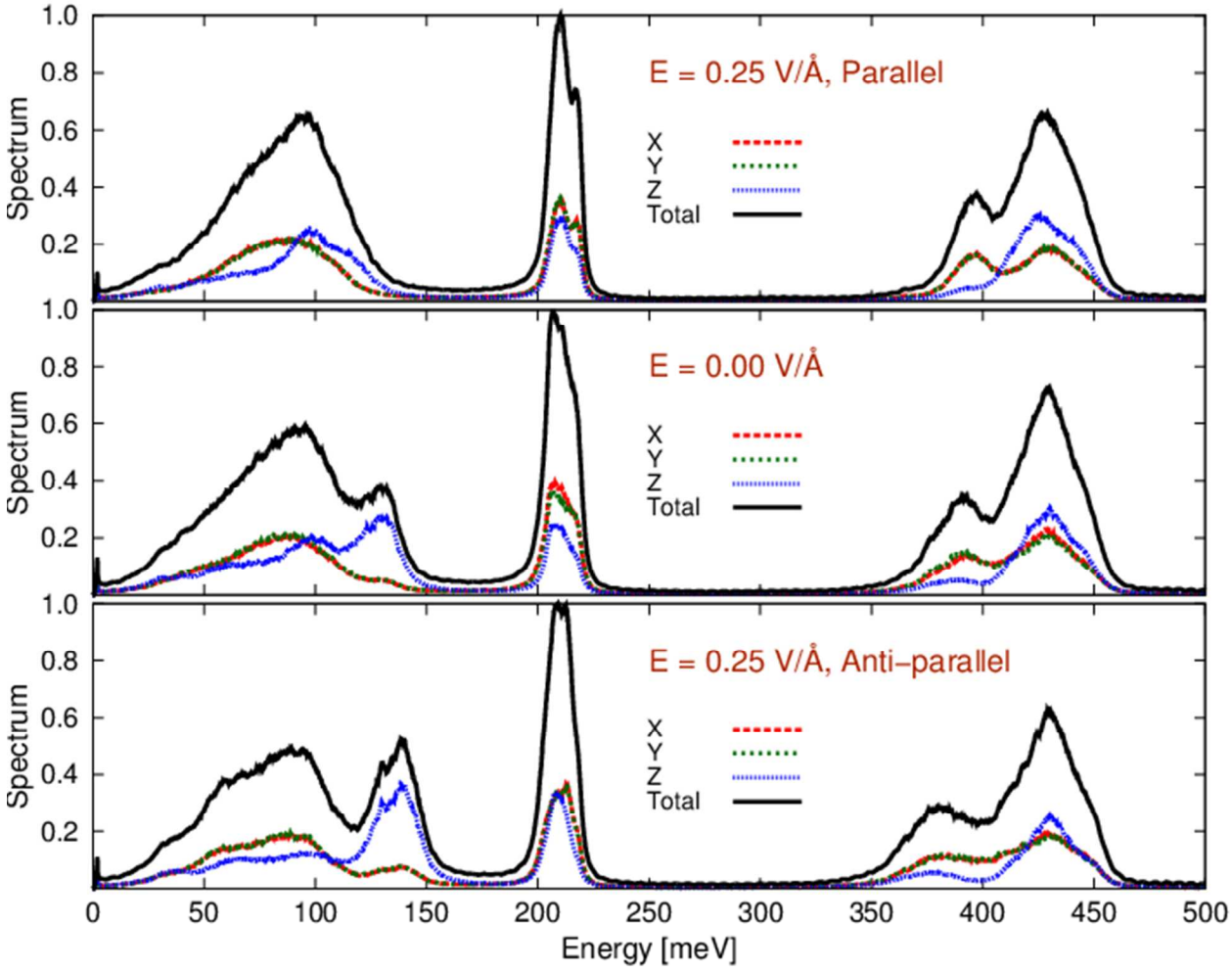

Figure S20: IR spectra of interfacial water on rutile (001) surfaces. Effects of the external static electric fields in the *z*-direction perpendical to the TiO_2 surface, parallel and antiparallel to the surface normal, are compared with the zero-field conditions. The spectra are decomposed to simulation-cell coordinate system.

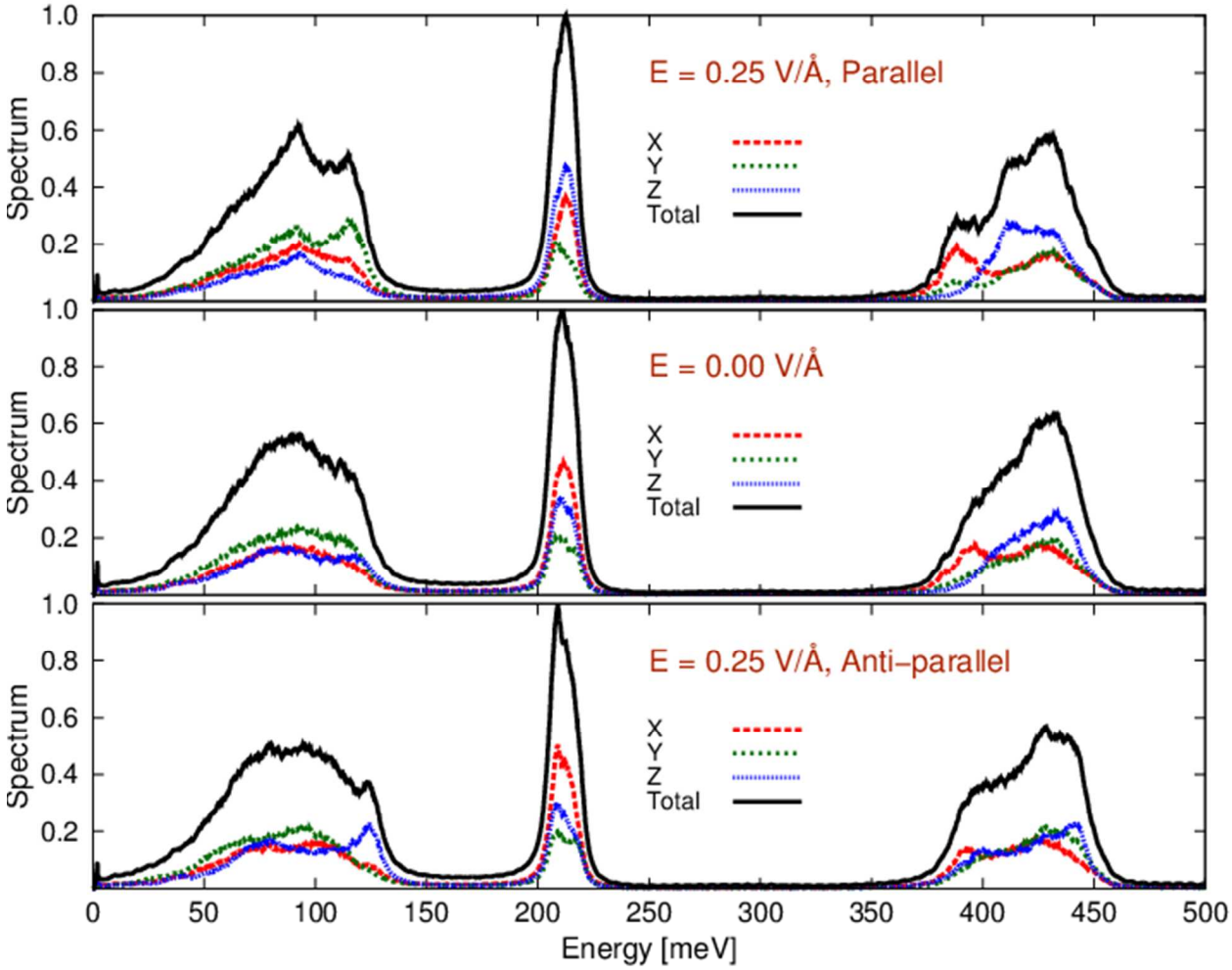

Figure S21: IR spectra of interfacial water on rutile (100) surfaces. Effects of the external static electric fields in the *z*-direction perpendical to the TiO_2 surface, parallel and antiparallel to the surface normal, are compared with the zero-field conditions. The spectra are decomposed to simulation-cell coordinate system.

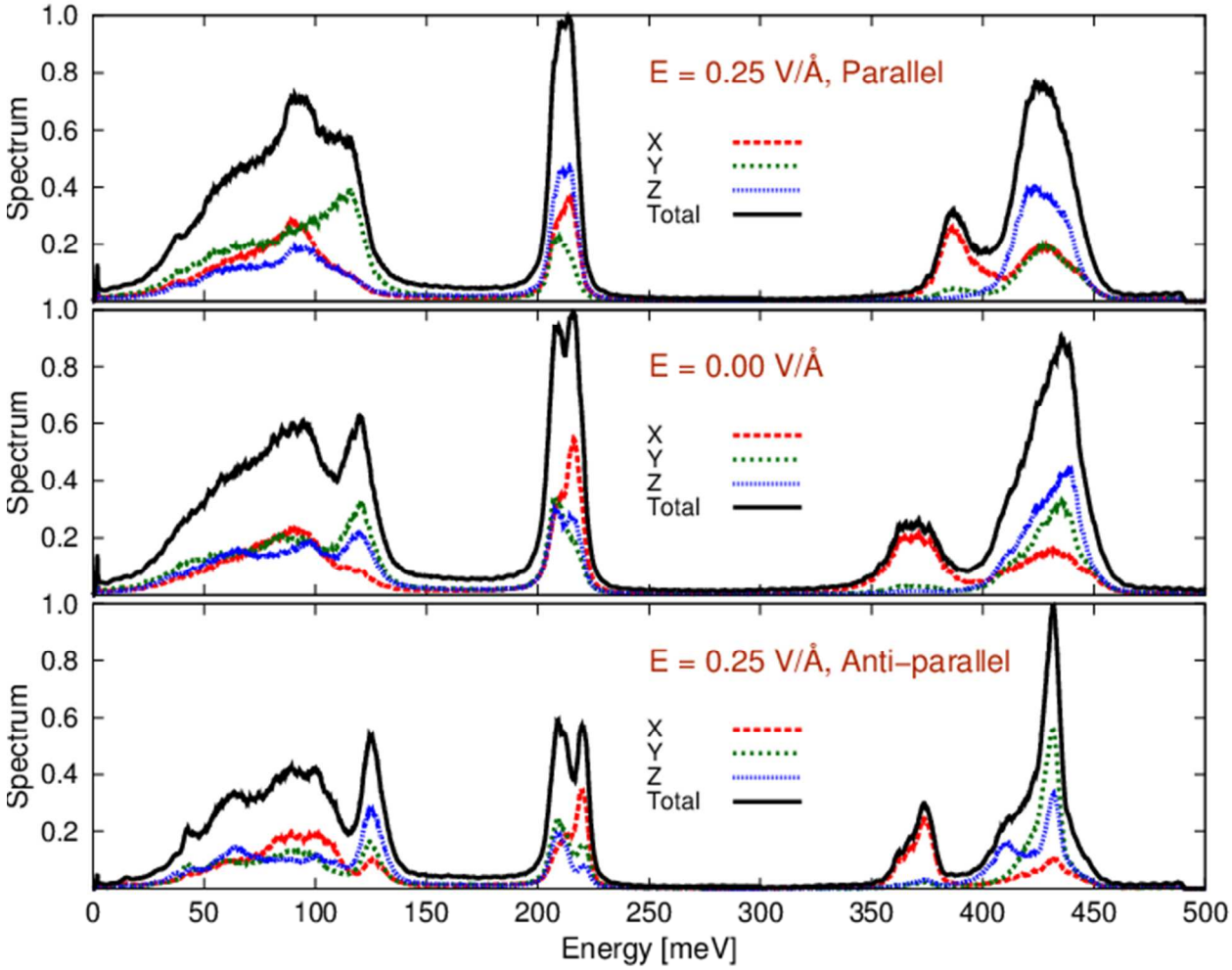

Figure S22: IR spectra of interfacial water on rutile (101) surfaces. Effects of the external static electric fields in the *z*-direction perpendical to the TiO_2 surface, parallel and antiparallel to the surface normal, are compared with the zero-field conditions. The spectra are decomposed to simulation-cell coordinate system.

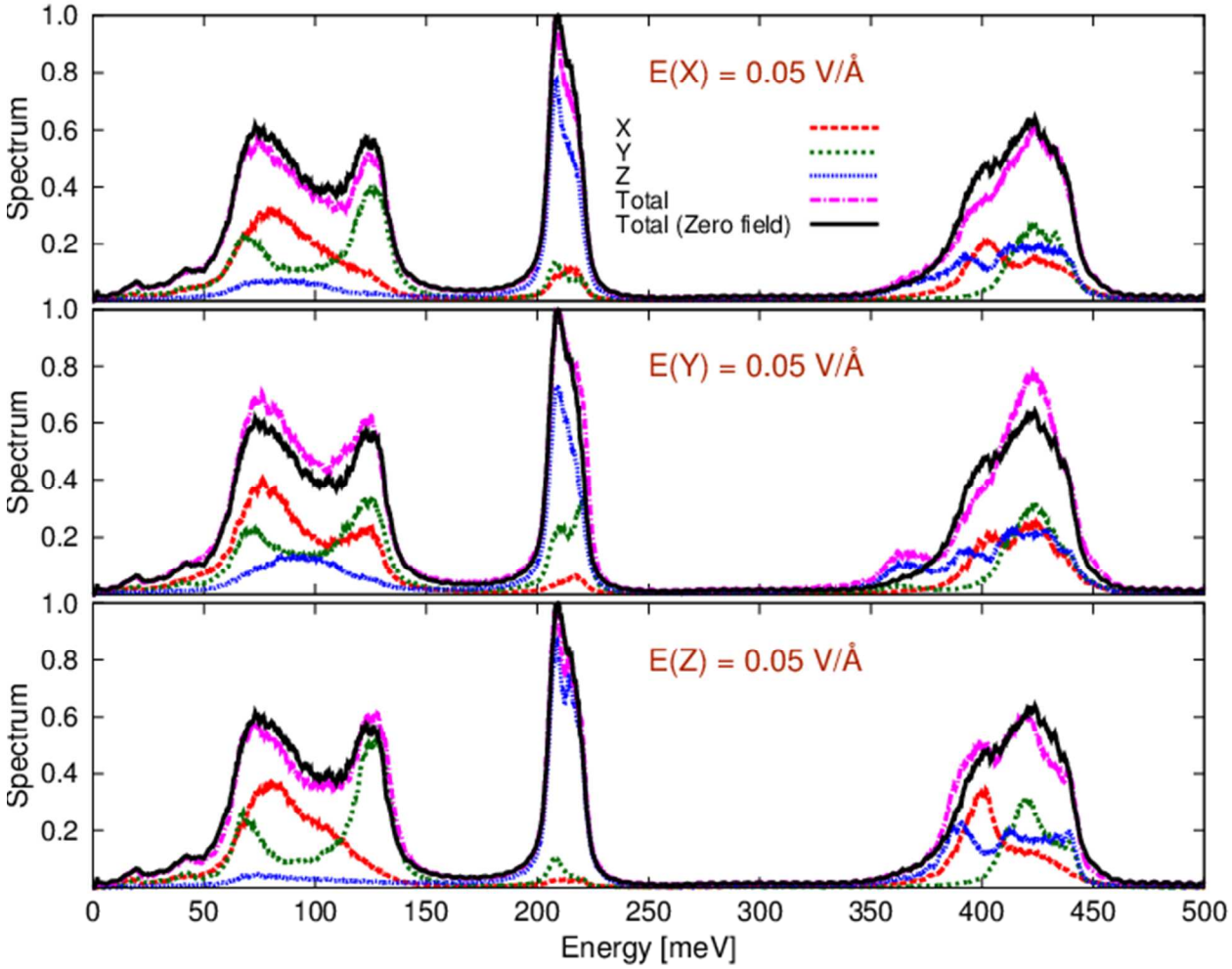

Figure S23: Effect of static electric field of 0.05 V/Å magnitude, applied in *x*, *y* and *z* direction corresponding to cell vectors, on IR spectra of anatase (101) interfacial water.

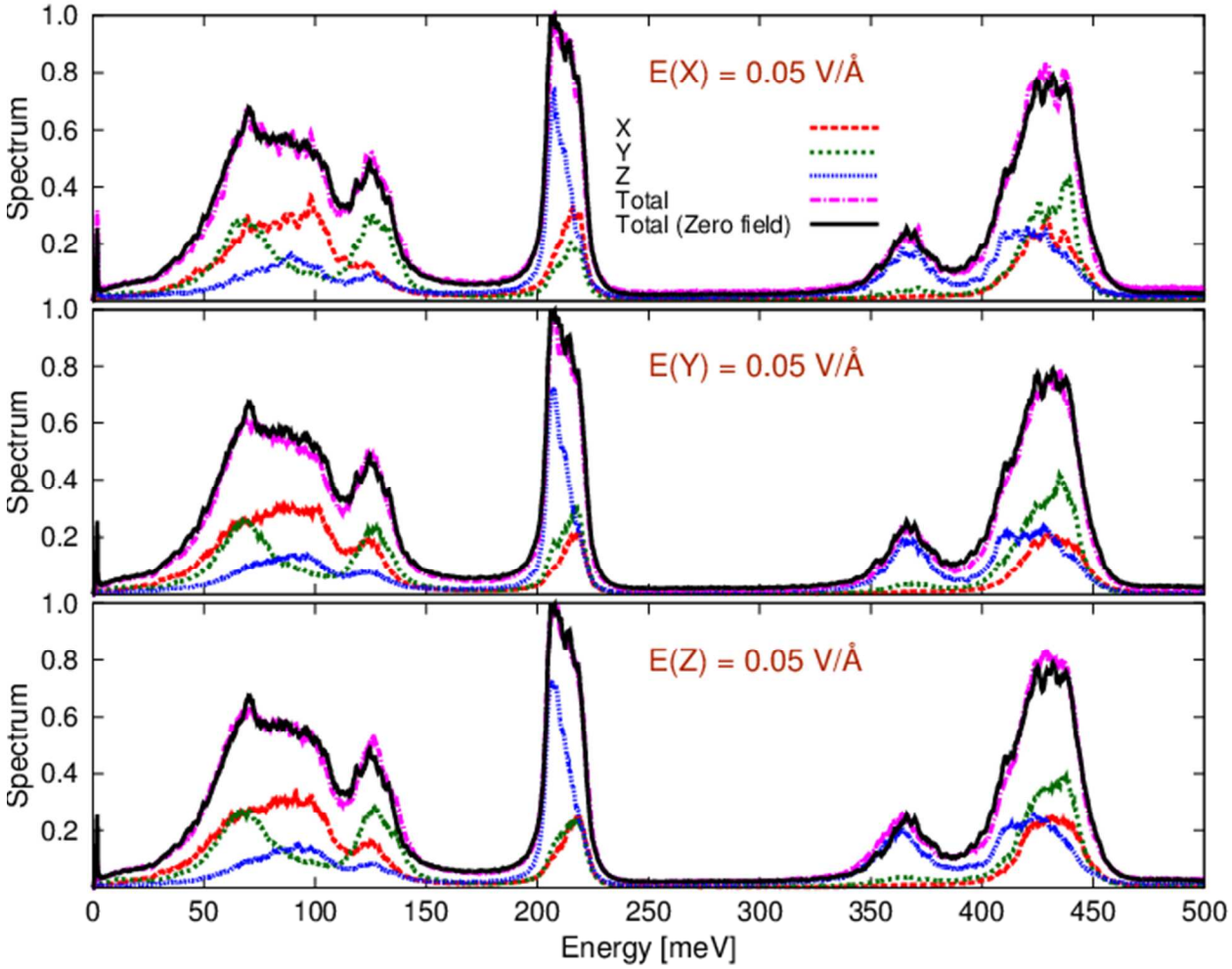

Figure S24: Effect of static electric field of 0.05 V/Å magnitude, applied in *x*, *y* and *z* direction corresponding to cell vectors, on IR spectra of rutile (110) interfacial water.